Comparison of high performance hybrid variable reluctance fast steering mirrors

René Rüddenklau*
Institute of Communications and Navigation
German Aerospace Center (DLR)
Weßling, Germany
rene.rueddenklau@dlr.de
*Corresponding author

Andreas Sinn
Automation and Control Institute
Technische Universität Wien
Vienna, Austria

Georg Schitter
Automation and Control Institute
Technische Universität Wien
Vienna, Austria

***Abstract*—Actuated mirrors are a key element in free-space optical communications. This paper compares the two high performance, commercially available actuators with a hybrid variable reluctance drive principle. They feature a mechanical range of up to 3 degrees and achieve closed-loop bandwidths of more than 1 kHz in combination with eddy-current sensors. It is shown, that the choice of driver is closely linked to their achievable dynamics. In particular, the performance in the application area of optical communication on satellites is analyzed. Therefore, in addition to the dynamic properties, the integration, their power consumption and suppression of vibrations is also being considered. To ensure comparability, a parameter tuning algorithm is used. The breadboard utilizes the same control software and hardware for both devices. The FSM20B shows better passive rejection against external vibrations, a lower average power consumption, and allows the exchange of its angular sensors. The FSM3000 achieves a better steady-state jitter, features a larger operating range and is more compact in size with precalibrated, internal sensors.**

***Index Terms*—free-space optical communications, hybrid variable reluctance actuator, fast steering mirror, beam steering, acquisition and tracking**

I. Introduction

Free-space optical communications (FSOC) enables the transmission of data with higher throughput than conventional radio frequency technologies and allows to integrate new security protocols based on quantum key distribution. Due to laser beams with low divergence requirements, it is crucial to ensure precise pointing under all circumstances [1]–[4]. This raises the need for high bandwidth actuators with a steering range in the order of degrees, which can also operate in the environment of space applications, since constellations gain an ever increasing role to transfer large amount of data [5]. A wide variety of actuators for beam steering are available today. A dedicated type of actuator to accomplish this task is known as a fast steering mirror (FSM). Different FSM types rely on fundamentally different drive technologies, which have various design parameters, each with specific advantages and disadvantages.

One way to compare these technologies is to approach their Pareto front of the range-bandwidth product (RBP) using existing devices [6]. The established actuation technologies for piezoelectric, Lorentz force-based and hybrid variable reluctance (HVR) were analyzed. The authors conclude that the HVR technology is the least widespread to date, but outperforms the other actuator types in terms of its RBP. A review of fine pointing actuators additionally considers micro-electro-mechanical systems (MEMS) technologies. The qualitative comparison of the RBP within yields the same results [7].

One reason why the HVR technology, despite its superiority, has not yet become widespread can be deduced from a closer look at the working principle of such an actuator [8]. The drive coil acts as an electromagnet, attracting the moving ferromagnetic part with a force proportional to the square of the electric current. In a hybrid actuator of this type, a permanent magnet is introduced into the system to equalize the DC offset in a double reluctance actuator which would otherwise be continuously generated by the coils, thus reducing power consumption. Ultimately, the introduced permanent magnet creates itself an unstable system, which would lead to strong non-linearities especially with increasing air-gap sizes between mover and each of the stator parts. An elastic hinge is introduced, to counteract this negative stiffness, which also makes the system linear for a wider range of motion. Only a limited number of FSMs based on these technologies are available and the evaluation of their individual properties is necessary to understand their suitability for the envisaged application. Both of the FSM are made for the needs of FSOC and are designed to withstand also harsh environments given in space applications. Nevertheless, usage in other applications with a high demand on scanning frequencies [9] such as for medical devices as well as in production and manufacturing processes is relevant.

The first available FSM with HVR principle was presented in a paper [10] in 2018. It is commercially available by the company Demcon in the Netherlands. For the purpose of this work, an early production batch actuator with serial number FSM20B-007 from 2020 is used. The second FSM is distributed by the company Micro-Epsilon in Germany. The engineering prototype is described and characterized in a previous work [11]. However, the following comparison uses the slightly modified commercial prototype version for evaluation. Note that changes by the manufacturers, in particular improvements in the design of both actuators, could be made at any time.

The main contribution of this paper is a dynamic analysis and comparison of the state of the art HVR FSM actuators, with an emphasis on their application to FSOC. It therefore extends on previous contributions by carying out all the analysis for both FSM in the same environment and the same hardware setup. This work includes a comparison of the design specifications, followed by a presentation of the test bench setup. Then the influence of the driver design is analyzed before the system identification and the controller design are performed. The power consumption in idle mode and in dynamic search mode, which occurs during the acquisition phase of optical links, is measured. To evaluate the validity of the controller design, the resonance shift of the FSM at the off-center position is evaluated. The implemented controller is then characterized for both systems by analyzing the steady-state jitter for different closed-loop bandwidths. Finally, the behavior under the influence of external vibrations, such as those that may occur in the satellite due to the use of reaction wheels, is studied.

II. System characterization

In Figure 1, both devices are displayed. It can be seen that both FSMs feature mounting ears to attach to a mount. Both mirror surfaces are in front of the mounting points. The sensor targets of the FSM20B are part of the mirror carrier, resulting in a shape with bulges, whereas a commercial of the shelf (COTS) mirror can be used with the FSM3000.

A. Specification

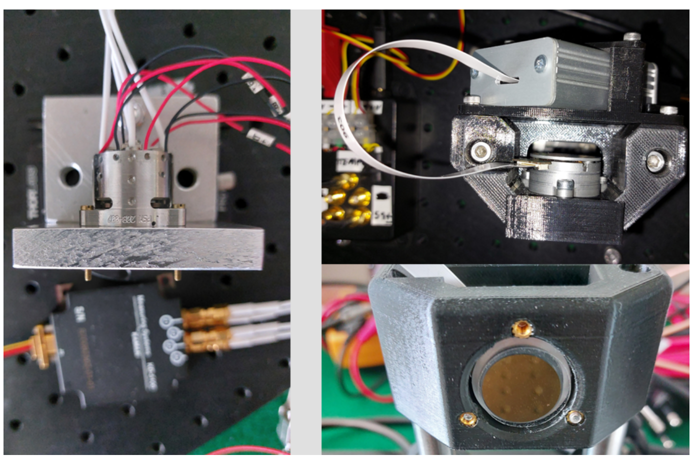

Fig. 1: The FSM20B from Demcon (left) and the FSM3000 from Micro-Epsilon (right).

It is noticeable that the FSM20B uses multiple cables for the drive and sensor lines, whereas the FSM3000 uses a flat, flexible cable. The application of FSOC demands that the cable length should be customizable, especially in the space sector with limited size capacity. The FSM20B uses twice as many actuation lines, since it features redundant coils for actuation. On the one hand, the FSM3000 offers the advantage that the sensor and actuator are supplied from a single source and thus, feature a small form factor. On the other hand, the bending direction of the supply cable is restricted due to the flex cable design.

Another aspect that is closely related to the actuator is the design of the necessary sensor electronics which, in both cases relies on eddy-current sensors (ECS). Models from Kaman and Lion Precision have already been tested with the FSM20B. Both were able to demonstrate comparable performance in the application and differ mainly in their hardware components and shape. The sensors of the FSM3000 are integrated within the FSM and do not need an additional assembly step for the integration into the end user application. Neither of the sensor companies provides a reference design for implementing the readout electronics into customized printed circuit boards. However, the manufacturers offer support for the use in space constraint systems. Important key specifications are presented in Table I.

TABLE I: Specification as provided by the manufacturer (unless otherwise stated) for the two analyzed FSM.

Property	**FSM20B**	**FSM3000**	**Unit**
Tip/tilt range	±1.0	±1.5	deg
End stop	±1.5	±2.5	deg
1st Resonance	120	70-80	Hz
Sensor bandwidth	20[b]	10-20	kHz
Clear aperture	20	20	mm
Angle sensors	third-party[b]	integrated	-
Envelope	Ø27x30	Ø25.5x19	mm
Coating	protected gold	protected gold	-
Random vibration	15[a]	40	gRMS
Sine vibration	25[a]	25	g
Sensor connector	third-party[b]	Micro-D[c]	-
Actuator connector	D-Sub	Micro-D[c]	-

[a] DLR internal testing for project related qualification.
[b] In this test Kaman KD-5100 sensors were used.
[c] Shared connector.

B. Hardware setup and real-time system

To control the FSMs, two identical hardware setups are used. Their basic structure is shown in Figure 2. They are implemented with a field programmable gate array (FPGA) based real-time system (Zedboard, Digilent, USA), which provides communication via user datagram protocol (UDP) to a computer for data recording, reference trajectory generation and control of the overall system. The coils of the FSMs are driven by custom-made, analog, closed-loop current amplifiers based on OPA549 (Texas Instruments, USA) operational amplifiers. They are designed for low-noise operation and feature a 16 bit digital to analog converter (DAC) to provide the reference signals for the PI-current controllers. The controllers are parametrized to match the electrical properties of the individual FSM coils and to achieve a closed-loop bandwidth of 16.49 Hz. The positions of the FSMs are measured by ECS which are read by a 24 bit analog to digital converter (ADC). The transformation to angular units is implemented on the Zedboard, as well as the position feedback controller. The sampling frequency of the system is 32 kHz with a dead-time of two samples due to the used ADC.

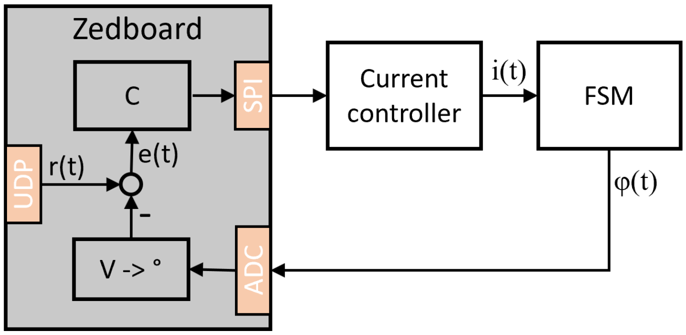

Fig. 2: Block diagram of the closed-loop system used for both FSMs, which was implemented on an FPGA-board shown in Figure 7.

The hardware setup described is used throughout the analysis process. The process itself consists of different aspects related to the application of free-space optical communication, which will be described in more detail in the following.

Before evaluating the FSM, a suitable driver must be found (see Section II-C). Therefore, the dynamic response function of a linear driver and a closed-loop driver is compared using a waveform generator to perform a chirp and by simultaneously measuring the coil current with a current clamp connected to an oscilloscope. As a second step, the current measurement setup is used to monitor the current consumption during operation. Since in applications such as FSOC on CubeSats, strict power budgets must be adhered to.

To characterize the FSM, the Zedboard is used to command a chirp and record the data simultaneously. Matlab is then used to generate an estimated frequency response and spectrum through a spectral analysis for the linear model. The dead time of the system is subsequently incorporated by multiplying the found model, as demonstrated in Section II-D. For additional information, the chirp command is applied at various offsets to determine any change in the resonant frequency. Massive variations would lead to a mismatch between the plant used for controller design and the actual dynamics, and can therefore have a severe impact on stability.

The following control design in Section III-A uses a PID controller implemented on the same Zedboard. The goal is to analyze the stability as well as the remaining jitter of the FSM in a static and controlled environment. This is the baseline for the Section III-B where both FSM are perturbed by external vibrations. The controller implementation and commanding is exactly the same as in the static case, but additional jitter could be measured that could not be compensated by the control loop. This scenario is important for satellites, which emit micro-vibrations that can interfere with the actuator and thus add to the pointing jitter.

C. Driver comparison

In the course of this analysis, the influence of the driver design in relation to closed-loop performance (see Sec. III-A) is evaluated. Two types of driver are being considered. The first is built upon a linear voltage to current converter and the second features an active current feedback loop. Both were examined in terms of their bandwidth (see Fig. 3). The open loop driver with connected load was measured to be a linear $0.0304\,\mathrm{AV}^{-1}$ driver and has its $-3\,\mathrm{dB}$ cutoff frequency at about $2.49\,\mathrm{kHz}$. Results showed that using the FSM20B, the current controlled driver allowed higher actuation bandwidth with comparable tracking error magnitudes. Therefore, for the following analysis both actuators were driven by the same closed-loop current driver.

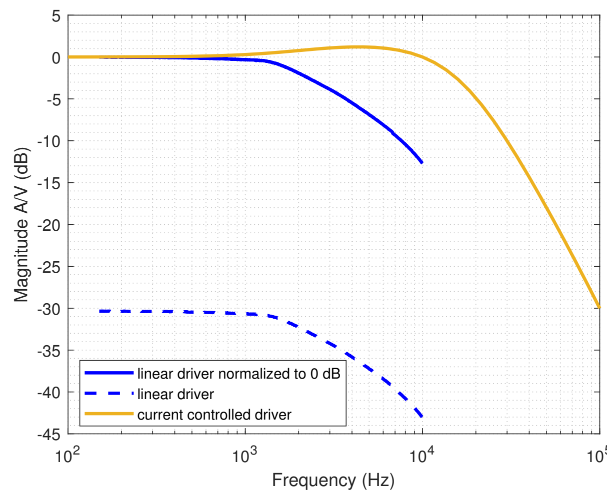

Fig. 3: Frequency response of the linear class A/B prototype driver and the closed-loop current controlled driver as developed by the Automation and Control Institute (ACIN).

Power consumption is another crucial aspect for FSOC applications on small satellites. Lower draining of the battery capacities contributes to increased availability of the laser communication terminal for data links. The following Table II summarizes the measured power in the idle state and during a spiral scan over the control range of ± 1 degree with a repetition rate of 8 seconds and 1.6 seconds respectively. The spiral scan is commonly used during the acquisition phase of an optical link in order to search in the field of uncertainty for the beacon of the link partner. The FSM3000 consumes more power ranging from 20% in standby to 39.5% more during fast spiral scanning. After evaluating the preferred driver, it can be proceeded with the analysis of the FSM plant characteristics. This step is essential to parameterize a controller for closed-loop operation.

TABLE II: Measured mean power consumption including drive electronics.

Mode	**FSM20B, W**	**FSM3000, W**	**ΔW, %**
Idle	3.00	3.60	20.0
8.0 secs period	3.52	4.64	31.8
1.6 secs period	3.67	5.12	39.5

D. System Identification

In order to identify the plant dynamics, and ultimately to design a closed-loop controller, it is crucial to measure magnitude and phase response. Both FSMs require processing to align the sensor with the actuator coordinate system. For the FSM3000, calibration parameters are provided by the manufacturer, whereas the FSM20B sensors are only calibrated to a dummy reference target at the third-party manufacturer. Therefore, no calibration between the optical axis and the measured mechanical axis exists. A 45 degree rotation is equally necessary to align the axis of the actuator with the differential ECS pair. The system dynamics are identified using a chirp input signal to the system while measuring the excitation with the internal sensors. The derived transfer function is of second order with a dead time term t_d of the form

$$G(s)_{FSM} = K \cdot \frac{\omega_0}{s^2 + 2\zeta\omega_0 s + \omega_0^2} \cdot e^{-t_d s}, \qquad (1)$$

where K is the gain, ω_0 is the natural frequency, ζ is the damping factor and s the complex Laplace variable. The FSM20B in Figure 4a shows a suspension mode of 119 Hz. The axes crosstalk suppression is 50 dB or better outside the resonance range of 90 Hz to 200 Hz and therefore, well decoupled. Both actuator phases show a latency that is visible in the t_d variable, corresponding to approximately four delay cycles of the digital system. The FSM3000 in Figure 4b shows a suspension mode at 72 Hz and the first structural mode around 2230 Hz. The axes crosstalk suppression is 40 dB or better outside the resonance range between 50 Hz and 90 Hz and therefore, also well decoupled. A summary of the estimated continuous plant transfer function parameters is given in Table III.

TABLE III: Transfer function parameters at FSM center.

Model	ω_0**, Hz**	K**, deg/A**	ζ	t_d**, secs**
FSM20B ϕ_1	119.2	36.57	0.0191	$130 \cdot 10^{-6}$
FSM20B ϕ_2	117.6	34.80	0.0199	$130 \cdot 10^{-6}$
FSM3000 ϕ_1	71.7	49.20	0.0288	$120 \cdot 10^{-6}$
FSM3000 ϕ_2	70.6	51.77	0.0298	$120 \cdot 10^{-6}$

Due to the design of HVR actuators, flexure mechanisms acting as a spring are installed internally as discussed in Section I. While the mirror platform is tilted to one side or the other, the effective stiffness of the system changes [8]. As a result, a shift of the suspension frequency does occur. As available controller implementations exploit this resonance frequency to enable faster scan trajectories and to save power consumption [9], it is of interest to know that characteristic frequency. A sensitivity analysis was performed, which runs the system identification process described above at different current offset values to bias the center position. Table IV reveals that FSM3000 appears to be less susceptible to changing offset positions.

III. System operation

After characterizing the system with the same hardware and environmental conditions, an operational scenario with closed-

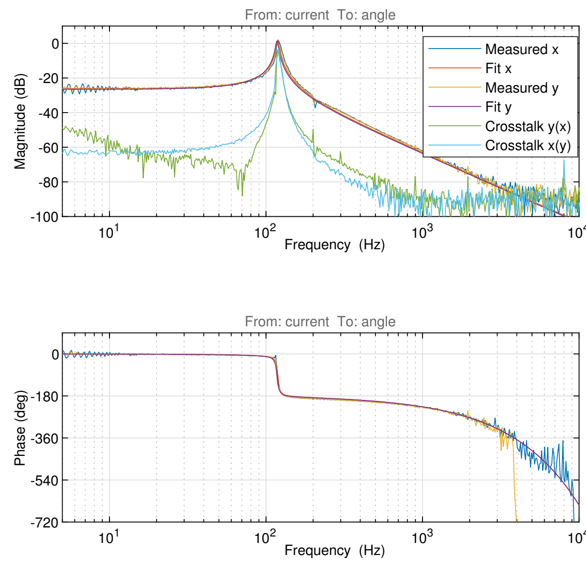

(a)

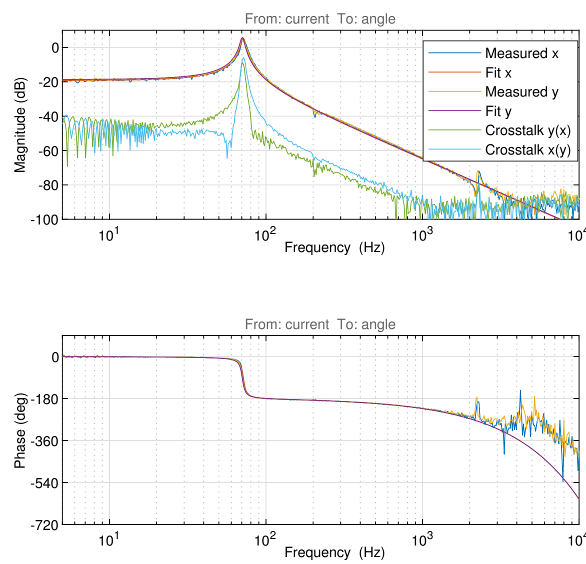

(b)

Fig. 4: Measured chirp response as estimated frequency domain data and identified system response for (a) FSM20B and (b) FSM3000.

TABLE IV: Eigenfrequency shift at selected offset currents.

Offset current, A	**FSM20B, Hz**	**FSM3000, Hz**
0.00	119	72
0.05	115	72
0.10	110	71
0.20	106	70

loop control is investigated. To ensure the same prerequisites, the same software was used to implement the controller. Moreover, a parametric PID controller tuning algorithm was used to ensure that the same tuning process is applied to each device under test (DUT).

A. Closed-loop performance and controller tuning

The mentioned tuning process was proposed for the parameterization of an FSM PID controller. It uses two degrees of freedom for tuning and allows a bandwidth orientated tuning process. The two design parameters are the crossover frequency ω_c and a tuning parameter α that controls the trade-off between performance and robustness. Following this concept, the controller transfer function $C(s)$ can be derived as

$$C(s) = \frac{1}{\alpha \cdot G(j\omega_c)} \left(1 + \frac{\omega_c}{\alpha^2 s} + \frac{\alpha}{\omega_c(\frac{s}{\alpha \cdot \omega_c} + 1)} s\right), \quad (2)$$

using the inverse of the FSM plant gain at the targeted crossover frequency [12].

Figure 5 shows the closed-loop sensitivity and complementary sensitivity functions which depict the disturbance rejection and the reference tracking behavior over the frequency range respectively. The envisaged 1 kHz bandwidth was achieved with $\omega_c = 365$ and $\alpha = 3$ for FSM3000 and $\omega_c = 350$ and $\alpha = 3$ for FSM20B. A stability analysis leaves a gain margin of 2.2 for both FSM as well as a phase margin of 28.5 degrees for the FSM20B and 30.1 degrees for the FSM3000. The so called *waterbed effect* [8] is visible in both complementary sensitivity graphs. It is a result of the unstable resonance frequency of the plant's open-loop transfer function. Another visible characteristic is the notch in the sensitivity function, which is at the suspension frequency of each system that supports superior suppression through its high gain factor.

In order to understand the 1σ jitter per axis of each device with respect to the closed-loop control bandwidth, discrete evaluation points were measured around the design bandwidth. The minimum measured closed-loop tracking setpoint jitter at 1 kHz bandwidth for FSM20B was 6.6 µrad and for FSM3000 3.2 µrad (see Fig. 6). Both FSM show that improved performance comes with increased jitter until the system becomes unstable. While both FSM do achieve bandwidths of more than 1 kHz and have measured standard deviations of a few microradians, it is still open how they behave under external disturbances.

Therefore, one scenario that is analyzed in the following section is their susceptibility to vibrations, which are present on the satellite due to onboard mechanisms such as mechanically tunable optical filters, crycoolers, solar array drive mechanisms, antenna pointing mechanisms, or reaction wheel assemblies [13].

B. Vibration rejection under application conditions

A test bench is set up to measure the response of the two systems to externally excited vibrations (see Fig 7). The control and data acquisition of the FSM and its sensors is

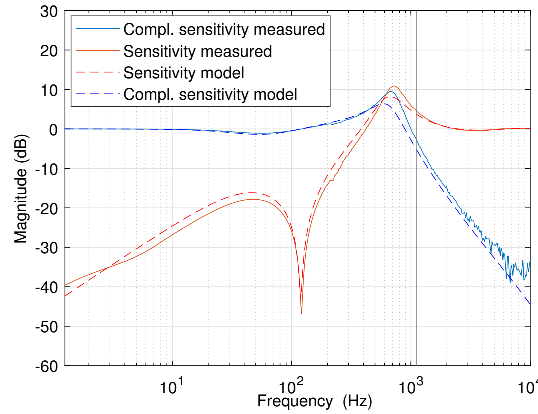

(a)

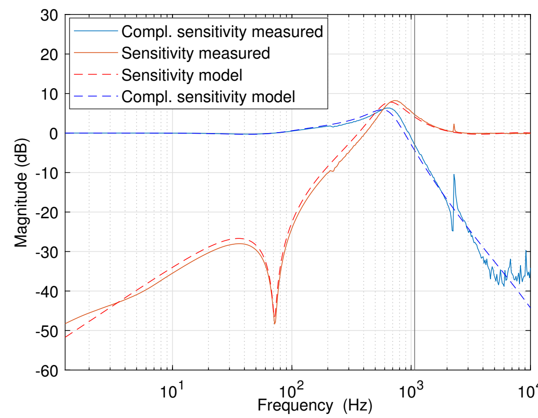

(b)

Fig. 5: Identification of the closed-loop transfer function for FSM20B (a) and FSM3000 (b).

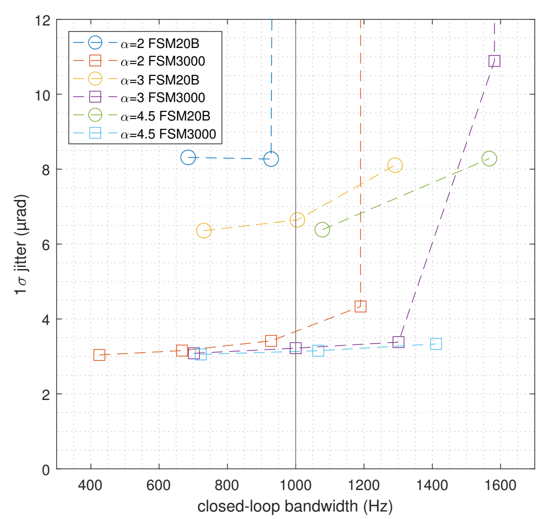

Fig. 6: Measured standard deviation at center tracking setpoint around the design bandwidth of 1 kHz.

done with the same hardware as used in Section II-D. The actuator of the shaker (TIRA TV 51110) is also controlled via the analog voltage output of the FPGA peripherals. A vibrometer (OFV-534) is installed to measure the velocity of the DUT in order to evaluate the commanded spectrum. This ensures that both DUT received the same excitation levels. The largest source of vibration on satellites are usually

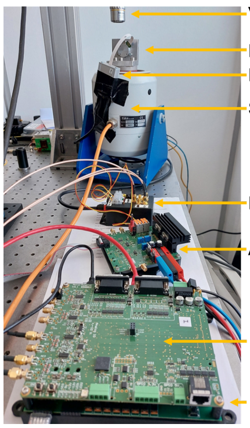

Fig. 7: Shaker test bench with mounted FSM and real-time controller hardware (see Sec. II-B).

the reaction wheels, used for attitude control, because they exhibit manufacturing-related imbalances [13]. The larger the satellite is, the greater vibration levels $[S] = \mathrm{gRMS}$ can be expected. In this test, two different spectra with $0.45\,\mathrm{gRMS}$ and $1.17\,\mathrm{gRMS}$ and constant magnitude over the range of $20\,\mathrm{Hz}$ - $2000\,\mathrm{Hz}$ are considered. As the spectrum depends heavily on the particular application, and amplification or attenuation can occur due to surrounding components and structures, this analysis should be repeated for the intended specific use case by the reader. However, the intention of this analysis is to enable a comparison under the same conditions and thus provide an indication of the susceptibility to vibration.

Measured are the open loop (OL) jitter and closed loop jitter (CL) during the same spectrum with mean value μ and standard deviation σ in Table V. When comparing the results

TABLE V: Vibration excitation measurement results for both axes ϕ_1 and ϕ_2.

S, gRMS	**FSM20B** (ϕ_1, ϕ_2)		**FSM3000** (ϕ_1, ϕ_2)	
	μ, **µrad**	1σ, **µrad**	μ, **µrad**	1σ, **µrad**
0.00 (OL)	n/a	$(5, 5)$	$(3714, 620)$	$(3, 4)$
0.00 (CL)	$(0, 0)$	$(6, 10)$	$(0, 0)$	$(3, 3)$
0.45 (OL)	n/a	$(15, 16)$	$(3710, 622)$	$(53, 310)$
0.45 (CL)	$(0, 0)$	$(5, 10)$	$(0, 0)$	$(3, 13)$
1.17 (OL)	n/a	$(75, 78)$	$(3710, 688)$	$(271, 1485)$
1.17 (CL)	$(0, 0)$	$(7, 14)$	$(0, 0)$	$(6, 45)$

of the two models, it is noticeable that the FSM20B shows a lower deviation from the mean in the unregulated case. As a result, the control also has to provide less high suppression due to already existing passive damping, which gives it an advantage. The mean value must be considered separately. As the FSM3000 already has a factory calibration of the sensor to the mirror axis, the absolute value can be used here. The FSM20B, on the other hand, is supplied uncalibrated in that sense. The angle measurements must therefore be regarded as relative. For the sake of simplicity, the zero value is set to the current mirror position each time the system experiences a power cycle.

C. Summary

Both FSMs are recommended for the use in FSOC applications, as they achieved satisfying results in all tests. This is demonstrated above all by the closed-loop disturbance rejection capabilities, which enable stabilized steering (see Fig. 8), even in challenging conditions. However, both devices come with their own advantages and disadvantages in direct comparison.

Fig. 8: Qualitative comparison of open-loop (left) and closed-loop (right) jitter under external vibration using two logos reflected from an external monitor on the mirror surface. Displayed is the FSM3000 with $0.45\,\mathrm{gRMS}$.

The FSM20B convinces with the following aspects:

- Stiffer due to a higher ω_0 frequency (see Tab. III), and thus, providing better passive resistance in the tested vibration environment compared to FSM3000 (see Tab. V),
- Lower average power consumption in the evaluated modes (see Tab. II),
- Redundant actuation coils (see Sec. II-A),
- Sensors are interchangeable with different vendors depending on the requirements, but it is the responsibility of the user to ensure proper alignment and calibration (see Tab. I).

These properties make it suitable for the intended application. The FSM3000 excels in:

- Lower steady-state jitter at $1\,\mathrm{kHz}$ bandwidth according to both internal sensors (see Fig. 6),
- Broader actuation range of ± 1.5 degrees (see Tab. I) and similar dynamics throughout that (see Tab. IV),
- Higher active suppression of vibration is possible, due to dynamics visible in transfer function (see Fig. 4a,4b,5a,5b),

- Internal sensors which are precalibrated with respect to the optical surface (see Sec. II-A).

It is therefore suitable for the envisioned application with the highest RBP [6] currently available for the group of COTS actuators under consideration.

IV. Conclusion

The focus of this work is to provide a comparison of available COTS HVR FSM with respect to their application in FSOC on satellites. Both FSM are tested with the same hardware and software configuration. Both prove that they belong to the high-end segment of the commercial market and set new benchmarks for the range-bandwidth-product in their actuator class. The FSM20B from Demcon compensates up to ± 1 degree of mechanical angle, whereas the FSM3000 from Micro-Epsilon allows up to ± 1.5 degrees range. Both are capable of reaching the design target bandwidth of 1 kHz. An improvement of bandwidth for both mirrors is possible by using a closed-loop current driver instead of a linear, open-loop voltage amplifier. Both actuator designs do suppress cross axis coupling so that a SISO controller can be implemented for tip and tilt. After close examination, both are suitable for FSOC space applications. A decision toward one of the models depends on the exact definition of the mission requirements and is at the discretion of the user.

Acknowledgment

The authors would like to thank Han Woong Yoo for the setup of the shaker and related discussions.

This work was supported by a mobility grant provided by the International Office of TU Wien.

Parts of the project on which this report is based was funded by the German Federal Ministry of Education and Research under the funding code 16KIS1079 and 16KIS1265. The authors are responsible for the content of this publication.

References

[1] R. Rüddenklau, E. Peev, and F. Moll, "Development of a cascaded fine pointing and tracking control loop for quantum key distribution via free-space optical communications," in *Environmental Effects on Light Propagation and Adaptive Systems V*, K. Stein and S. Gladysz, Eds. SPIE, 05.09.2022 - 08.09.2022, p. 12. [Online]. Available: https://www.spiedigitallibrary.org/conference-proceedings-of-spie/12266/2636111/Development-of-a-cascaded-fine-pointing-and-tracking-control-loop/10.1117/12.2636111.full

[2] H. Kaushal and G. Kaddoum, "Optical communication in space: Challenges and mitigation techniques," *IEEE Communications Surveys & Tutorials*, vol. 19, no. 1, pp. 57–96, 2017.

[3] M. Toyoshima, "Trends in satellite communications and the role of optical free-space communications [invited]," *Journal of Optical Networking*, vol. 4, no. 6, p. 300, 2005.

[4] V. Vaishali and S. Sancheti, "Investigation between performances of free space optical communication links under atmospheric turbulence," *Journal of Communications*, pp. 368–374, 01 2018.

[5] A. U. Chaudhry and H. Yanikomeroglu, "Laser intersatellite links in a starlink constellation: A classification and analysis," *IEEE Vehicular Technology Magazine*, vol. 16, no. 2, pp. 48–56, 2021.

[6] E. Csencsics and G. Schitter, "Exploring the pareto fronts of actuation technologies for high performance mechatronic systems," *IEEE/ASME Transactions on Mechatronics*, vol. 26, no. 2, pp. 1053–1063, 2021.

[7] M. Milaševičius and L. Mačiulis, "A review of mechanical fine-pointing actuators for free-space optical communication," *Aerospace*, vol. 11, no. 1, p. 5, 2024.

[8] R. Munnig Schmidt, G. Schitter, A. Rankers, and J. van Eijk, *The design of high performance mechatronics: High-tech functionality by multidisciplinary system integration*, third revised edition ed. Amsterdam: Delft University Press, 2020. [Online]. Available: https://ebookcentral.proquest.com/lib/kxp/detail.action?docID=6143718

[9] E. Csencsics and G. Schitter, "System design and control of a resonant fast steering mirror for lissajous-based scanning," *IEEE/ASME Transactions on Mechatronics*, vol. 22, no. 5, pp. 1963–1972, 2017.

[10] G. Witvoet, S. Kuiper, and A. Meskers, "Performance validation of a high-bandwidth fine steering mirror for optical communications," in *International Conference on Space Optics — ICSO 2018*, Z. Sodnik, N. Karafolas, and B. Cugny, Eds., vol. 11180, International Society for Optics and Photonics. SPIE, 2019, p. 1118061. [Online]. Available: https://doi.org/10.1117/12.2536136

[11] E. Csencsics, J. Schlarp, T. Schopf, and G. Schitter, "Compact high performance hybrid reluctance actuated fast steering mirror system," *Mechatronics*, vol. 62, p. 102251, 2019. [Online]. Available: https://www.sciencedirect.com/science/article/pii/S0957415819300571

[12] E. Csencsics and G. Schitter, "Parametric pid controller tuning for a fast steering mirror," in *2017 IEEE Conference on Control Technology and Applications (CCTA)*. IEEE, 2017, pp. 1673–1678.

[13] D.-K. Kim, "Micro-vibration model and parameter estimation method of a reaction wheel assembly," *Journal of Sound and Vibration*, vol. 333, no. 18, pp. 4214–4231, 2014.